World Academy of Science, Engineering and Technology
International Journal of Electrical and Information Engineering
Vol:16, No:8, 2022

An Effective Noise Resistant FM Continuous-Wave Radar Vital Sign Signal Detection Method

Lu Yang, Meiyang Song, Xiang Yu, Wenhao Zhou, Chuntao Feng

***Abstract*—**To address the problem that the FM continuous-wave (FMCW) radar extracts human vital sign signals which are susceptible to noise interference and low reconstruction accuracy, a detection scheme for the sign signals is proposed. Firstly, an improved complete ensemble empirical modal decomposition with adaptive noise (ICEEMDAN) algorithm is applied to decompose the radar-extracted thoracic signals to obtain several intrinsic modal functions (IMF) with different spatial scales, and then the IMF components are optimized by a backpropagation (BP) neural network improved by immune genetic algorithm (IGA). The simulation results show that this scheme can effectively separate the noise, accurately extract the respiratory and heartbeat signals and improve the reconstruction accuracy and signal-to-noise ratio of the sign signals.

***Keywords*—**Frequency modulated continuous wave radar, ICEEMDAN, BP Neural Network, vital signs signal.

I. Introduction

VITAL signs can indicate the severity and criticality of a patient's condition, and real-time detection of human sign information is significant in areas such as smart homes and smart healthcare [1]-[3]. Currently, available devices for contact detection of vital signs are large, costly, and complex to operate [4], while non-contact radar detection methods, in addition to their user-friendly advantages, provide an effective method for situations where optical imaging is obstructed, such as poorly lit sleeping environments and cramped spaces under wastelands caused by earthquake disasters [5]. Among the major non-contact radar detection technologies available today, Ultra-Wide Band (UWB) pulsed radar [6] is superior in terms of distance resolution and detection capability, but its complex structure leads to high cost. Continuous-wave (CW) radar [7] cannot measure distance and is susceptible to interference from echoes of surrounding moving targets. Compared with the above detection methods, the high-resolution and high-precision FMCW [8]-[10] combines the advantages of continuous-wave and ultra-wideband radar with low power, high sensitivity, and high penetration, and can accurately measure the target and clutter characteristics, and provide the target's distance, velocity and angle information of the target.

The vital signals obtained by radar include not only the signals of physical signs but also various kinds of clutter interference, and the respiratory harmonics will interfere with the frequency components of the heartbeat, and the higher-order harmonics of respiration will also be confused with the heartbeat signal, so the extraction and separation of cardiopulmonary signals face a considerable challenge. The empirical mode decomposition (EMD) algorithm and BP neural network for vital sign signal detection scheme proposed in the literature [11] can extract respiratory and heartbeat signals, but due to the modal confounding and endpoint effects in the decomposition results of EMD, and the BP neural network is easy to fall into the local minimum resulting in the accuracy of the final optimized reconstructed signal is not satisfactory. To address the above problems, an ICEEMDAN algorithm is proposed to overcome the modal aliasing and decompose the signal more thoroughly and efficiently, which can effectively separate noise and accurately extract respiratory and heartbeat signals and the BP neural network is improved by IGA to overcome the local minimum, search for the global optimal solution, and optimize the intrinsic mode function (IMF) to achieve high accuracy detection and reconstruction of the sign signal under noise interference.

II. FMCW Radar Detection Principle

Human breathing and heartbeat cause regular movements of the chest cavity. The radar transmits electromagnetic wave signals through the antenna to the person to be tested, and the reflected echo from the surface of the chest cavity of the person to be tested contains background, redundant cluster, etc. The time-frequency diagram of the FMCW radar emission and echo signals is shown in Fig. 1.

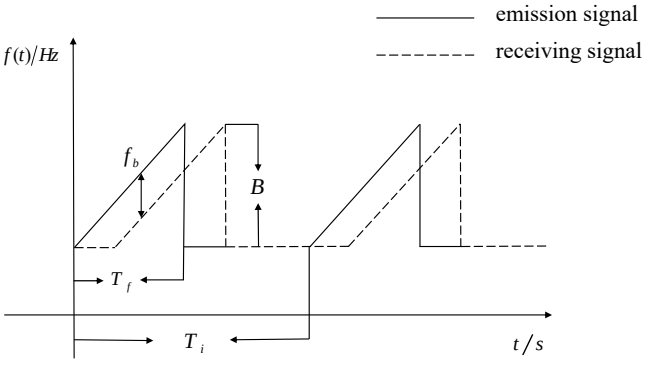

Fig. 1 FMCW radar transmit signal and echo signal

The transmit signal of the FMCW radar can be expressed as:

$$x_T(t) = A_T \cos(2\pi f_c t + \pi \frac{B}{T_c} t^2 + \theta(t)) \quad (1)$$

Lu Yang, Meiyang Song, Xiang Yu, Wenhao Zhou and Chuntao Feng are with School of Communication and Information Engineering, Chongqing University of Posts and Telecommunications, Chongqing, China (e-mail: 1434564011@ qq.com).

where A_T is the transmitting power and $\theta(t)$ is the transmitter phase noise. Some relevant chirp parameters are defined as follows: f_c is the chirp start frequency, B is the chirp signal bandwidth, T_f is the chirp signal period, T_i is the transmit signal frame period, and T_c is the chirp signal duration.

We assume that $x(t)$ is the micro-motion displacement of the thorax, d_0 is the distance between the radar sensor and the body. Then, the distance between the thorax and the radar is $R(t) = x(t) + d_0$, the delay is $t_d = 2R(t)/c$, and c is the speed of light. We express the signal received by the radar by:

$$x_R(t) = A_R\{\cos(2\pi f_c(t-t_d)) + \pi\frac{B}{T_c}(t-t_d)^2 + \theta(t-t_d)\} \tag{2}$$

The transmit signal and the return signal are mixed through a quadrature I/Q channel, and then a low-pass filter is used to obtain the intermediate frequency (IF) signal of the radar $S_{IF}(t)$.

$$\begin{aligned} S_{IF}(t) &= A_{IF}\exp(j(2\pi[\frac{B}{T_c}t_d]t + 2\pi f_c t_d + \pi\frac{B}{T_c}t_d^{\,2} + \Delta\theta(t))) \\ &\approx A_{IF}\exp(j(2\pi[\frac{B}{T_c}t_d]t + 2\pi f_c t_d + \Delta\theta(t))) \\ &\approx A_{IF}\exp(j(\frac{4\pi BR(t)}{cT_c}t + \frac{4\pi R(t)}{\lambda}) \\ &\approx A_{IF}\exp(j(2\pi f_b t + \varphi_b(t)) \end{aligned} \tag{3}$$

where, $\lambda = c/f_c$ is the wavelength of the millimeter wave, f_b is the IF signal frequency, $\varphi_b(t)$ is the IF signal phase, and its expression is:

$$f_b = \frac{2BR(t)}{cT_c} \tag{4}$$

$$\varphi_b(t) = \frac{4\pi R(t)}{\lambda} \tag{5}$$

The frequency and phase of the radar IF signal are proportional to the tiny motion of the chest surface, and analog to digital (A/D) sampling of the IF signal is performed to obtain the raw radar data. A distance dimensional Fourier transform, also called range fast Fourier transform (FFT), is performed on the n chirp signals from the radar to obtain a complex matrix M [m, n], where m is the number of Fourier points. Each column represents a distance unit, consisting of m units, where the unit with the largest magnitude is the measured object. The phase information of the target distance unit is extracted, and the phase deconvolution is performed to obtain $\varphi(t)$, and obtain the differential signal, and the phase baseline drift due to hardware reasons is eliminated by phase differencing, and then the signal processing of $\Delta\varphi$ is performed to obtain the vital sign information.

III. Noise-Resistant Vital Signs Detection Solution Design

A. Noise-Resistant Separation Algorithm for Breathing and Heartbeat

The application of FMCW radar for human vital sign detection inevitably involves noise such as background and redundant clutter. ICEEMDAN, as an improvement of CEEMDAN decomposition algorithm, can overcome the problems of noise residue after decomposition and false patterns at the early stage of decomposition, so its design can be applied to the detection of vital signs signals to achieve the extraction and separation of respiration and heartbeat signals, and the redundant noise can be removed. The algorithm is applied to the detection of millimeter-wave radar vital signs signal to achieve the separation of signal and noise in four steps. We define operator E(.) to represent the IMF component of the signal obtained by EMD decomposition, operator M(.) to represent the local average of the sought signal, $W_{(i)}(t)$ denotes the i th zero-mean Gaussian white noise added, β_0 is the amplitude factor of the added noise, and $<.>$ denotes the set total average of the sought signal. The input signal $x(t)$ is the original thoracic signal acquired by the radar. The specific implementation process of the algorithm is as follows.

Step1. Gaussian white noise decomposed by EMD is added to the original thorax signal acquired by radar, for which the local mean and set total average are obtained for the first stage (k = 1) signal residual r_1 and the first-order model.

$$x^{(i)}(t) = x(t) + \beta_0 E_1(W^{(i)}(t)) \tag{6}$$

$$r_1(t) = \left\langle M(r^{(i)}(t))\right\rangle = \left\langle M(x(t) + \beta_0 E_1(W^{(i)}(t)))\right\rangle \tag{7}$$

$$IMF_1 = x(t) - r_1(t) = x(t) - \left\langle M(x(t) + \beta_0 E_1(W^{(i)}(t)))\right\rangle \tag{8}$$

Step2. We continue to add the EMD-decomposed Gaussian white noise to the above residual signal, find its local means as the second stage (k = 2) residual r_2 and find the second-order model.

$$r_2(t) = \left\langle M(r_1 + \beta_1 E_2(W^{(i)}(t)))\right\rangle \tag{9}$$

$$IMF_2 = r_1(t) - r_2(t) = r_1(t) - \left\langle M(r_1 + \beta_1 E_2(W^{(i)}(t)))\right\rangle \tag{10}$$

Step3. For k = 3..., K calculates the kth residual.

$$r_k(t) = \left\langle M(r_{k-1} + \beta_{k-1} E_k(W^{(i)}(t)))\right\rangle \tag{11}$$

$$IMF_k = r_{k-1}(t) - r_k(t) = r_{k-1}(t) - \left\langle M(r_{k-1} + \beta_{k-1} E_k(W^{(i)}(t)))\right\rangle \tag{12}$$

Step4. We repeat step 3 until the residual component $r_k(t)$ is monotonic or can no longer be decomposed. If the

thoracic signal $x(t)$ can be decomposed into N IMF components, then $x(t)$ can be expressed as in:

$$x(t)=\sum_{k=1}^{N} IMF_k(t)+r_N(t) \tag{13}$$

The algorithm decomposes the raw chest signal $x(t)$ acquired by the radar into several modal functions of different frequencies and a residual component. In general, the respiratory frequency of a healthy person ranges from 0.2 Hz to 0.8 Hz, and the heart rate ranges from 0.8 Hz to 2 Hz. Therefore, by finding the spectral peaks of the decomposed IMF components, the components belonging to the respiratory signal and the components belonging to the heartbeat signal can be determined separately, and the rest is noise.

B. IGA-BP to Extract Vital Signs Signals

The ICEEMDAN algorithm can effectively separate noise and accurately extract respiration and heartbeat signals, but the separated IMF components suffer from endpoint effects and cannot avoid bias in reconstructing the target signal. To obtain IMF components with better performance, they must be optimized to improve reconstruction accuracy while maintaining signal characteristics.

The application of neural networks for feature extraction is currently a widely adopted method. The topology of the BP neural network is shown in Fig. 2, and the basic idea of this network model is to use BP to analyze the deviation of the output and expectation of each training result, to dynamically adjust the weights and thresholds of each node, and finally to obtain a model whose output is consistent with the expected result, minimizing the sum of squares of the network deviation. Although this algorithm has good nonlinear mapping performance, its convergence speed is slow, the training network is unstable, and the modification rule of weights and thresholds is the fastest descent method, which also leads to the generation of multiple local minima making it into local minima and a long learning period [12]. Therefore, the application of the BP neural network to the vital signs radar signal decomposed using the ICEEMDAN algorithm to achieve the desired signal extraction still needs to overcome the above problems, for which the IGA-BP optimization strategy is proposed.

IGA-BP is to introduce the IGA genetic algorithm into the BP neural network to screen out individuals with better environmental adaptation ability in each generation of genetic inheritance and use genetic reworking technique for crossover and variation to obtain a new set of approximate solutions to optimize the weights and thresholds of the BP neural network, which can not only avoid immature convergence, but also find the optimal solution in the global. The IGA-BP optimization strategy is shown in Fig. 3, and its flow is as follows.

a) Build a BP neural network with initial network weights and thresholds.
b) Sequentially encode the initial weights and thresholds of the network.
c) Input the IMF dataset obtained from ICEEMDAN decomposition to train the BP neural network and find the fitness value of each chromosome based on the output error and fitness function.
d) Select the individuals with higher fitness to perform the crossover variation operation and find the maximum fitness value of each generation.
e) Reach the maximum evolutionary generation of the population and continue to perform the next optimization step, otherwise return to step c.
f) Decode the optimal chromosome to obtain the optimal weight threshold and assign it to the BP neural network.
g) Process the IMF data input in step c and give the optimal weight threshold to calculate the output deviation.
h) Update the threshold of the network according to the deviations by the gradient descent algorithm.
i) Reach the predetermined deviation accuracy or the proposed training number, the training is finished and the result is output, otherwise return to step g.

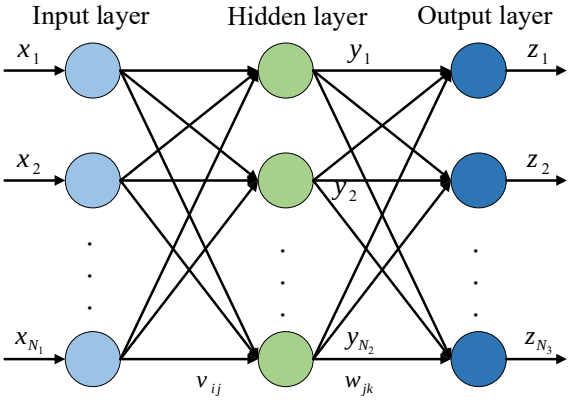

Fig. 2 BP neural network topology

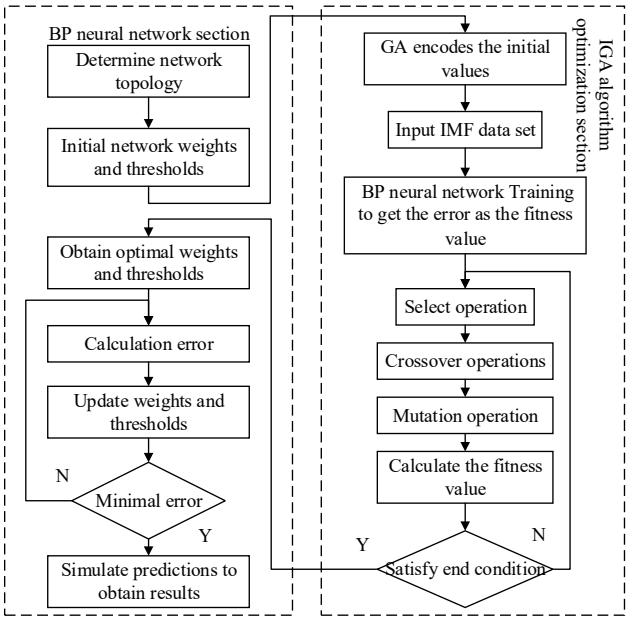

Fig. 3 Workflow of BP neural network based on genetic algorithm

The initial weights and thresholds of the neural network are optimized to finally achieve the goal of optimizing the IMF components decomposed by ICEEMDAN to improve the accuracy and precision of respiratory and heartbeat signal reconstruction. The optimized BP neural network improves the network performance and not only finds the global optimal solution but also improves the accuracy of parameter extraction.

C. ICEEMDAN and IGA-BP Based Vital Signs Signal Detection Scheme

In summary, the proposed ICEEMDAN algorithm enables the separation of sign signals and noise, and the initial extraction of respiratory and heartbeat signals. And the IGA-BP is used to further optimize the IMF components obtained from the decomposition, to achieve the high-precision reconstruction of the respiratory and heartbeat signals. In this regard, the process design of combining the ICEEMDAN algorithm and IGA-BP applied to FMCW radar detection of vital signs signals is shown in Fig. 4. As can be seen from the figure, the raw signals collected by the radar are processed by ICEEMDAN and IGA-BP to finally obtain the respiration and heartbeat signals with high accuracy.

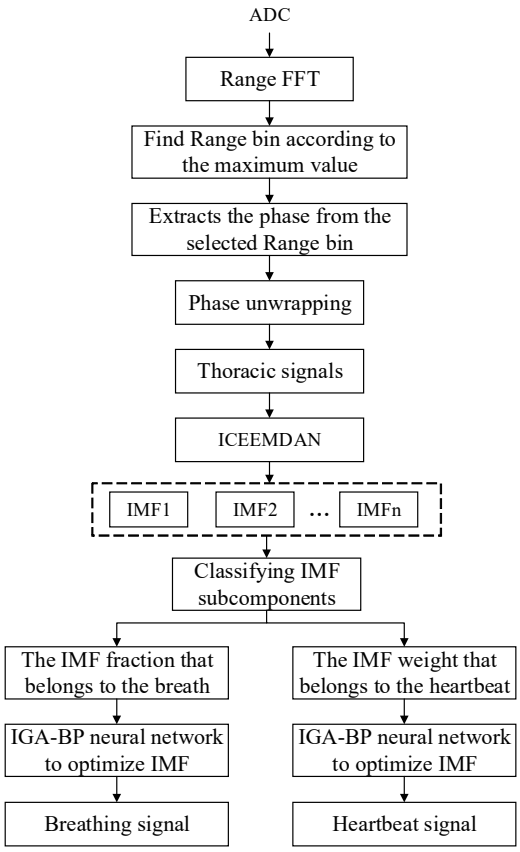

Fig. 4 Vital signs detection system process

IV. Analysis of Simulation Results

To suppress the effects of spectral noise and respiratory harmonics on the heartbeat signal and achieve high accuracy detection and reconstruction of the vital signs signal, the proposed ICEEMDAN combined with IGA-BP neural network radar detection scheme for vital signs signal is simulated and analyzed for verification. The 24 GHz millimeter wave radar module is used for chest data acquisition of indoor stationary targets. The specific parameters are shown in Table I. The experiments were performed by Python and MATLAB platform for signal processing and simulation analysis.

TABLE I
FMCW Radar Parameters

Parameters	Value
Starting frequency f_c	24 GHz
Bandwidth B	4 G
Frame period T_i	50 ms
Pulse duration T_c	50 us
Number of samples per chirp	100

A. Extraction of Vital Signs Signals

The distance information can be obtained by doing FFT on the raw radar data in chirp. As shown in Fig. 5, each chirp signal emitted by the radar does 256 points FFT, and the range FFT results in 128 points FFT to get the 3D model map of 2D FFT. The maximum amplitude point in the figure is the location of the measured target, and the detection result shows that the target is at rest, and the distance from the radar is about 59 cm.

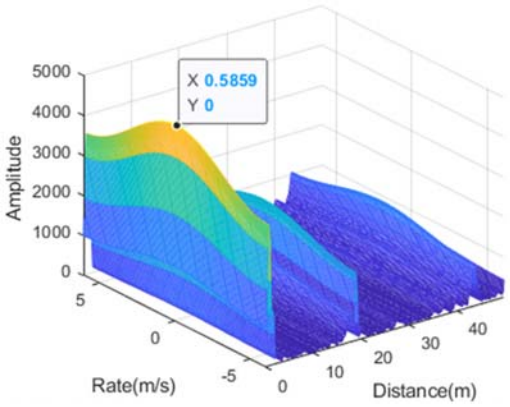

Fig. 5 Radar target detection results

B. Comprehensive Performance Analysis of Modal Decomposition Algorithm

The five algorithms, EMD, EEMD, CEEMD, CEEMDAN and ICEEMDAN, are simulated and analyzed in terms of four evaluation metrics: number of components, orthogonality, number of parameters and running time, respectively, as shown in Table II.

Comparing the data in Table II, it can be seen that EMD has the least human factor and better adaptivity, but poor orthogonality, while CEEMDAN and ICEEMDAN have good orthogonality and can effectively suppress modal mixing, although they have longer running time. Therefore, further simulation experiments on these two algorithms are conducted next to select the modal decomposition algorithm with the best separation effect and detection accuracy for subsequent

experiments.

TABLE II
PERFORMANCE COMPARISON OF DIFFERENT DECOMPOSITION ALGORITHMS

Algorithm	Number of components	Orthogonality	Number of parameters	Running time/s
EMD	7	1.192	1	1.042
EEMD	9	0.147	3	24.907
CEEMD	10	0.628	3	16.359
CEEMDAN	11	0.071	4	30.525
ICEEMDAN	9	0.025	4	32.618

C. Separation of Vital Signs Signals

Fig. 6 shows the heartbeat signal and its spectrum collected by the contact fingertip sensor as the reference signal for this experiment, which is compared with the heartbeat signal spectrum obtained from the decomposition of the CEEMDAN algorithm and ICEEMDAN algorithm to verify the superiority of the ICEEMDAN algorithm. As shown in Fig. 7, the CEEMDAN decomposition is performed to decompose the radar differential signal into 11 IMF components, at the early stage of signal decomposition, due to the existence of "spurious" modes, making the previous order mode contain a lot of noise and similar scales, and the decomposed IMF still contains residual noise, Fig. 8 shows the decomposition of ICEEMDAN yields 9 IMF components with higher decomposition efficiency and more single frequency, less clutter, and more concentrated energy. Separate FFT of the decomposed IMF components can be obtained with the corresponding spectrum, according to the spectrum peak judgment belongs to the IMF components of breathing and heartbeat, and the rest are noise interference components.

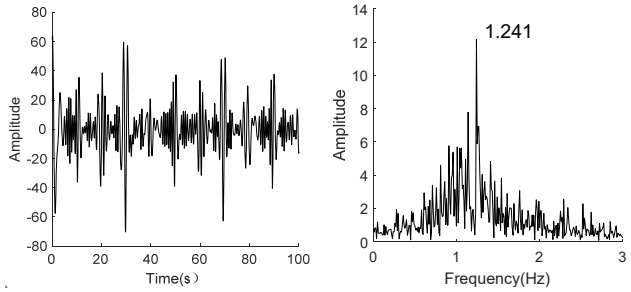

(a) Time domain (b) Frequency domain

Fig. 6 Heartbeat reference signal

The respiration and heartbeat signal spectra separated by the two algorithms are shown in Figs. 9 and 10, respectively. The respiration frequency obtained by the CEEMDAN decomposition method is 0.5869 Hz and the heartbeat frequency is 1.317 Hz, while the respiration frequency obtained by the ICEEMDAN decomposition method is 0.5869 Hz and the heartbeat frequency is 1.231 Hz. A comparison with the reference heartbeat frequency of 1.241 Hz in Fig. 6 (b) shows that the heartbeat signal extracted from the CEEMDAN decomposition results has a larger error, while the heartbeat signal extracted from the ICEEMDAN decomposition results is more accurate, with an error of only 1% compared to the results collected by the contact fingertip sensor.

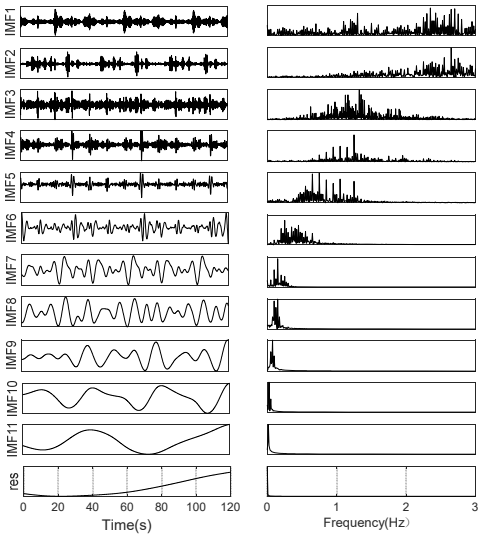

Fig. 7 CEEMDAN decomposition results

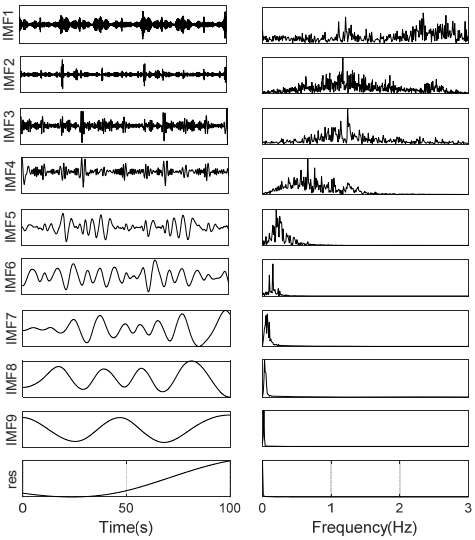

Fig. 8 ICEEMDAN decomposition results

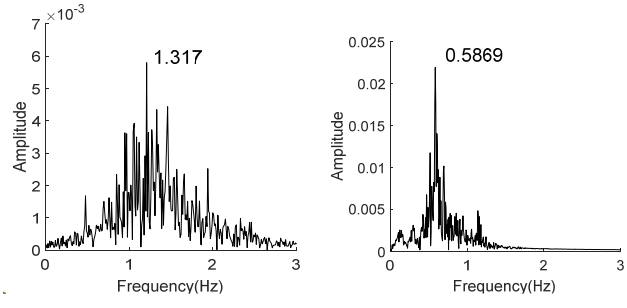

(a) Heartbeat signal spectrum (b) Respiratory signal spectrum

Fig. 9 CEEMDAN signal spectrum

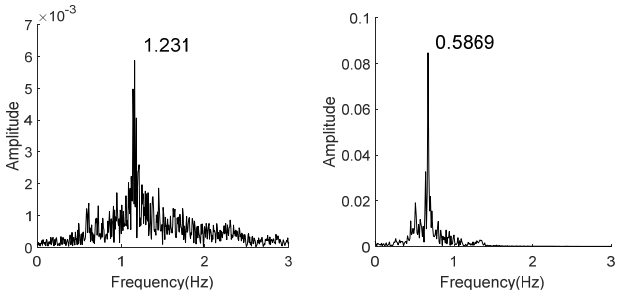

(a) Heartbeat signal spectrum (b) Respiratory signal spectrum

Fig. 10 ICEEMDAN signal spectrum

D. Reconstructing Vital Signs Signals

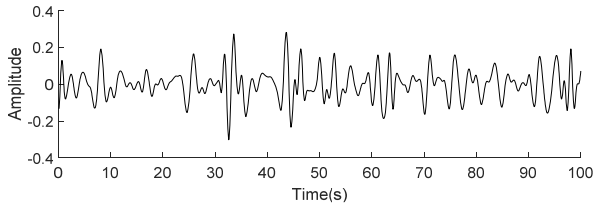

(a) Respiratory signal reconstructed by FFT

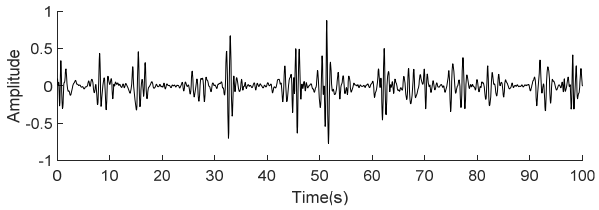

(b) Heartbeat signal reconstructed by FFT

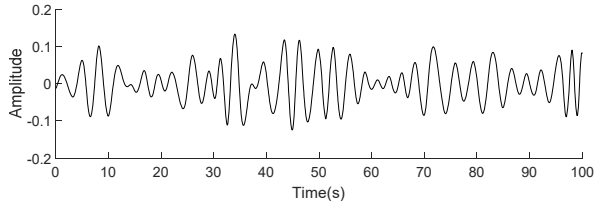

(c) IGA-BP optimized respiratory signal

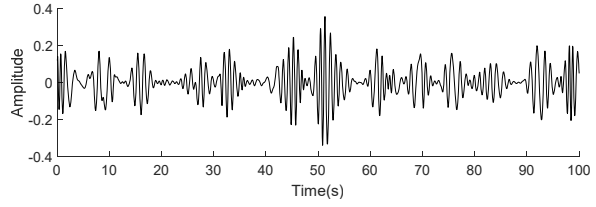

(d) IGA-BP optimized heartbeat signal

Fig. 11 IGA-BP comparison before and after optimization

The ICEEMDAN algorithm can achieve the separation of respiration, heartbeat, and noise signals, but the separated IMF components suffer from problems such as endpoint effects and cannot avoid errors when performing target signal reconstitution. To be able to obtain the IMF component with better performance, the proposed IGA-BP strategy to optimize the IMF performance is compared with the results before optimization as shown in Fig. 11. Figs. 11 (a) and (b) show the respiration and heartbeat signals reconstructed directly according to the spectrum peak, and (c) and (d) show the respiration and heartbeat signals reconstructed after the optimization of the IGA-BP strategy, respectively. From the waveforms, there are more spurious components and unclear features in the sign signals before optimization, and the endpoint effect still exists. In contrast, the waveforms optimized with the IGA-BP strategy can clearly reflect the characteristics of the respiratory and heartbeat signals and can well solve the shortage of end-jump.

E. Signal to Noise Ratio Comparison

The results and signal-to-noise ratios of the five subjects' vital signals acquired at 0.4 m, 0.6 m, and 1.2 m from the radar to perform ICEEMDAN decomposition, direct reconstruction, and IGA-BP optimization followed by reconstruction according to the spectrum analysis results are shown in Tables III-VI. SNR1 and SNR2 in the tables represent the signal-to-noise ratios of the respiratory and heartbeat signals respectively.

The signal-to-noise ratio is defined as follows:

$$SNR=10\lg\left(\frac{s^2(l)}{\sum s^2(f)-s^2(l)}\right) \tag{14}$$

where $s(l)$ is the peak of the spectrum of the signal, $\sum s^2(f)$ is the energy sum of the entire signal spectrum.

TABLE III
RESPIRATORY AND HEARTBEAT SIGNAL RESULTS AFTER FFT AND IGA-BP RECONSTRUCTION AT 0.4 M

Experimenter	Method	Breathing rate /Hz	SNR1 /dB	Heart rate /Hz	SNR2 /dB
A	FFT	0.31	-4.09	1.26	-7.36
	IGA-BP	0.31	-3.45	1.24	-4.78
B	FFT	0.54	-6.93	1.16	-5.83
	IGA-BP	0.48	-7.18	1.16	-6.36
C	FFT	0.42	-5.68	1.08	-4.84
	IGA-BP	0.45	-3.26	1.12	-3.32
D	FFT	0.25	-2.13	0.98	-10.73
	IGA-BP	0.32	-1.52	1.40	-8.15
E	FFT	0.37	-7. 84	1.37	-5.89
	IGA-BP	0.37	-9.16	1.37	-5.16

TABLE IV
RESPIRATORY AND HEARTBEAT SIGNAL RESULTS AFTER FFT AND IGA-BP RECONSTRUCTION AT 0.6 M

Experimenter	Method	Breathing rate /Hz	SNR1 /dB	Heart rate /Hz	SNR2 /dB
A	FFT	0.31	-4.09	1.26	-7.36
	IGA-BP	0.31	-3.45	1.24	-4.78
B	FFT	0.54	-6.93	1.16	-5.83
	IGA-BP	0.48	-7.18	1.16	-6.36
C	FFT	0.42	-5.68	1.08	-4.84
	IGA-BP	0.45	-3.26	1.12	-3.32
D	FFT	0.25	-2.13	0.98	-10.73
	IGA-BP	0.32	-1.52	1.40	-8.15
E	FFT	0.37	-7. 84	1.37	-5.89
	IGA-BP	0.37	-9.16	1.37	-5.16

TABLE VI
RESPIRATORY AND HEARTBEAT SIGNAL RESULTS AFTER FFT AND IGA-BP RECONSTRUCTION AT 1.2 M

Experimenter	Method	Breathing rate /Hz	SNR1 /dB	Heart rate /Hz	SNR2 /dB
A	FFT	0.31	-4.09	1.26	-7.36
	IGA-BP	0.31	-3.45	1.24	-4.78
B	FFT	0.54	-6.93	1.16	-5.83
	IGA-BP	0.48	-7.18	1.16	-6.36
C	FFT	0.42	-5.68	1.08	-4.84
	IGA-BP	0.45	-3.26	1.12	-3.32
D	FFT	0.25	-2.13	0.98	-10.73
	IGA-BP	0.32	-1.52	1.40	-8.15
E	FFT	0.37	-7. 84	1.37	-5.89
	IGA-BP	0.37	-9.16	1.37	-5.16

Comparing the experimental data, the signal-to-noise ratio of respiratory and heartbeat signals reconstructed by the IGA-BP method is significantly improved compared with that of the FFT direct reconstruction method, with an average increase of 1.24 dB for respiratory signals and 2.05 dB for heartbeat signals.

V. CONCLUSION

Aiming at the problems of spectral noise and harmonic interference in the detection of vital signs signals by FMCW radar and the low accuracy of reconstruction of signs signals, the ICEEMDAN combined with the IGA-BP neural network is proposed as a radar detection scheme for vital signs signals. The experimental simulation results show that this scheme can effectively separate the noise and accurately detect the human breathing and heartbeat signals, and the comparison results with contact instruments show that the heartbeat detection error is only 1%. The reconstructed signals after IGA-BP optimization have a good signal-to-noise ratio and improve the accuracy of the signal reconstruction, among which, the signal-to-noise ratio of respiration and heartbeat signals are improved by 1.24 dB and 2.05 dB on average.

REFERENCES

[1] Celler B G, Sparks R S. Home telemonitoring of vital signs—technical challenges and future directions (J). IEEE journal of biomedical and health informatics, 2014, 19(1): 82-91.
[2] Xie L, Tian J, Li H, et al. Wireless Healthcare System for Life Detection and Vital Sign Monitoring (C)//2020 IEEE 91st Vehicular Technology Conference (VTC2020-Spring). IEEE, 2020: 1-5.
[3] Zheng Hongmei, Ge Miao, Chen Ke, et al. Separation study of heartbeat signal and respiration signal based on FCEEMD (J). Journal of Electronic Measurement and Instrumentation, 2017, 31(11): 1809-1814.
[4] Yen H T, Kurosawa M, Kirimoto T, et al. Proof-of-principle Experiment on 24 GHz Medical Radar for Non-contact Vital Signs Measurement (C)//2021 43rd Annual International Conference of the IEEE Engineering in Medicine & Biology Society (EMBC). IEEE, 2021: 6884-6884.
[5] Chen W, Lan S, Zhang G. Multiple-Target Vital Signs Sensing using 77GHz FMCW radar (C)//2021 15th European Conference on Antennas and Propagation (EU CAP). IEEE, 2021: 1-3.
[6] Shen H, Xu C, Yang Y, et al. Respiration and heartbeat rates measurement based on autocorrelation using IR-UWB radar (J). IEEE transactions on circuits and systems II: express briefs, 2018, 65(10): 1470-1474.
[7] Zakrzewski M, Raittinen H, Vanhala J. Comparison of center estimation algorithms for heart and respiration monitoring with microwave Doppler radar (J). IEEE Sensors Journal, 2011, 12(3): 627-634.
[8] Fang G W, Huang C Y, Yang C L. Switch-based low intermediate frequency system of a vital sign radar for simultaneous multitarget and multidirectional detection (J). IEEE Journal of Electromagnetics, RF and Microwaves in Medicine and Biology, 2020, 4(4): 265-272.
[9] Sacco G, Piuzzi E, Pittella E, et al. Vital Signs Monitoring for Different Chest Orientations Using an FMCW Radar (C)//2020 XXXIIIrd General Assembly and Scientific Symposium of the International Union of Radio Science. IEEE, 2020: 1-4.
[10] Pal S. FMCW–Radar Design: by M. Jankiraman, London, ARTECH HOUSE, 2018, 415 pp., $179 (hardback), ISBN-13: 978-1-63081-567-7 (J). 2019.
[11] Cui LH, Zhao AX, Ning FZ. Radar sign signal detection algorithm based on EMD and BP neural network[J]. Computer System Applications, 2017, 26(8): 217-222.
[12] Xiao Jialin, Yue Dianwu, Zhao Zhengduo, et al. Genetic algorithm-based optimization of BP neural network for visible light localization (J). Optoelectronics - Laser, 2019, 30(8): 810-816.